Korchun A. V., Evshchik E. Yu., Baskakov S. A., Bushkova O. V., Dobrovolsky Y. A.
Chimica Techno Acta. 2020. Vol. 7, no. 4. P. 259–268.
ISSN 2409–5613

DOI: 10.15826/chimtech.2020.7.4.21

Influence of a binder on the electrochemical behaviour of Si/RGO composite as negative electrode material for Li-ion batteries

A. V. Korchun[a*], E. Yu. Evshchik[a], S. A. Baskakov[a], O. V. Bushkova[a,b], Y. A. Dobrovolsky[a]

[a] *Institute of Problems of Chemical Physics of the Russian Academy of Sciences, 1 Academician Semenov av., Chernogolovka, Moscow region, 142432, Russia*
[b] *Institute of Solid State Chemistry of the Ural Branch of the Russian Academy of Sciences, 91 Pervomaiskaya st., Ekaterinburg, Russia*
**email: andrei_korchun@mail.ru*

Abstract. A composite consisting of silicon nanoparticles and reduced graphene oxide nanosheets (Si/RGO) was studied as a promising material for the negative electrode of lithium-ion batteries. Commonly used polyvinylidene fluoride (PVdF) and carboxymethyl cellulose (CMC) served as a binder. To reveal the influence of the binder on the electrochemical behaviour of the Si/RGO composite, binder-free electrodes were also prepared and examined. Anode half-cells with composites comprising CMC as a binder demonstrated the best properties: capacity over 1200 mAh·g^{-1}, excellent cycling performance and good rate capability up to 1.0*C*.

Keywords: Li-ion battery; negative electrode; nanocomposite; reduced graphene oxide; silicon nanoparticles

Received: 02.12.2020. Accepted: 21.12.2020. Published:30.12.2020.

Introduction

Li-ion batteries (LIBs) are leading electrochemical energy storage systems among secondary batteries due to their high energy density. Graphite, the most common material of the negative electrode, is widely used in LIBs production for several reasons: good cyclability, low cost, non-toxicity, low operating voltage [1]. Commercial graphitised materials demonstrate specific capacity near 360 mAh·g^{-1} [2], which is very close to the limiting value of the theoretical capacity of graphite, 372 mAh·g^{-1}. Further improvements in the total capacity of LIBs require a material with a much higher capacity. Silicon is a promising material for the negative electrode due to its high theoretical capacity of 3579 mAh·g^{-1} (which corresponds to the formation of $Li_{3.75}Si$ compound [3]); it is almost ten times more than that of graphite. Unfortunately, individual macroscale silicon is not suitable for practical usage in LIBs as a negative electrode because of colossal volume changes during lithiation [4], causing cracks and leading to loss of material integrity [5]. Silicon nanoparticles can withstand such volume changes without destruction, but they still have low electronic and ionic conductivity. Moreover, the high surface area of Si nanoparticles leads to excessive solid-electrolyte in-

terphase (SEI) formation. All these peculiar properties hinder their application in LIBs as the negative electrode material [6].

A promising way to incorporate silicon into LIBs production is combining it with various carbonaceous materials (nanotubes, graphite, amorphous coatings, graphene and others) to obtain a composite [7]. Carbon enhances electronic and ionic transport throughout a composite and helps maintain material stability [8]. Choice of a binder also plays a significant role in the stability improvement of the silicon-containing electrode, providing good adhesion to the current collector and reliable contact with carbonaceous particles for better electronic conductivity [9, 10].

Reduced graphene oxide seems to be a suitable carbonaceous material to stabilize silicon nanoparticles during cycling and provide fast electron transfer in such a composite. Few recent works describe design and modification of Si/RGO composites to achieve better performance during cycling; some researchers tried to modify the silicon particle surface for better contact between Si and RGO [11–14]. For example, covering with poly(diallyl dimethylammonium chloride) which can change the surface charge of silicon to positive was studied [11]. Si/GO composite was assembled by electrostatic attraction, and then GO was reduced into RGO by heat treatment [11]. Another approach to stabilize the composite structure is to cover Si/RGO particles with pyrolyzed carbon [12, 13]. Other researches also use simple routes to obtain Si/RGO composites with good cycling stability [14].

In this work, a new approach to obtain Si/RGO composite was developed, and the influence of a binder on cycling behaviour of the Si/RGO composite was investigated.

Experimental

Starting materials

Graphene oxide water suspension with a concentration of 14.6 mg·cm^{-3} was provided by GRAPHENOX LLC (Russia). Silicon nanoparticles were prepared by the destruction of monosilane in argon plasma, as described in [15]; average particle size was 50 nm (SEM), and the specific area was 52 m^2·g^{-1} (by BET).

Composite preparation

Si/RGO composite with 50:50 ratio (by weight) was prepared by self-assembly in a water suspension. 100 cm^3 of GO suspension was ultrasonically dispersed for 5 minutes. Then, 774 mg of silicon nanoparticles were added to the suspension and again ultrasonically dispersed for 5 minutes. After that, the suspension was frozen in cylindrical moulds with an inner diameter of 20 mm on a copper plate cooled by liquid nitrogen. Finally, the frozen suspension was freeze-dried for 72 hours at –55 °C (Martin Christ Alpha 1–4 LDplus, Germany). The resulting aerogel was then reduced in hydrazine vapour atmosphere at room temperature and dried in an oven at 65 °C. Samples thus obtained were named as SiRGO.

Electrode preparation

Active mass of electrode consisted of Si/RGO composite and a binder (PVdF or CMC) at 90:10 ratio (by weight); electrode without binder was also prepared, for comparison. N-Methyl-2-pyrrolidone (NMP) was used as a solvent for samples with PVdF binder, and water was used as a solvent for samples with CMC binder. PVdF and CMC binders were purchased from Sigma-Al-

drich. Table 1 presents the type of polymer binder and the composition of electrode active mass. Samples without binder were designated as SiRGO1, with PVdF binder — as SiRGO2, and with CMC binder — as SiRGO3. The area of prepared electrodes was 2.25 cm^2. The active material loading of the electrode was about 0.5 $mg \cdot cm^{-2}$.

Table 1

Compositions of electrode active mass

Sample	Binder	Composite:binder ratio
SiRGO1	None	—
SiRGO2	PVdF	90:10
SiRGO3	CMC	90:10

Electrode slurry was prepared by adding a suitable solvent to a composite powder with further homogenization by IKA T10 Ultra Turrax equipment (10 min) and then by an ultrasonic bath (10 min). Electrode slurry without binder was prepared by adding NMP to a composite powder with subsequent homogenization as described above. Electrode slurry was applied onto a copper current collector using Dr Blade technology with subsequent calendering and vacuum drying at 120 °C for 12 h.

Methods

The morphology of the composite samples was studied by scanning electron microscopy (SEM) using Zeiss LEO SUPRA 25 (Germany) equipment with accelerating voltage of 12 kV.

Electrochemical characteristics of the Si/RGO composite electrodes with various binders were measured in two-electrode pouch cells modelling anode half-element of LIB. The cells were assembled in an argon-filled glove box. Lithium metal foil on a copper current collector served as a counter electrode, and a baseline 1 m solution of $LiPF_6$ in ethylene carbonate (EC)/ethyl methyl carbonate (EMC) mixture (1:1 by volume) served as an electrolyte; Celgard 2300 film served as a separator. The residual water content in the electrolyte solution did not exceed 30 ppm. All components were supplied by Sigma-Aldrich. Cyclic voltammetry (CV) and galvanostatic cycling (GST) were performed using a multi-channel potentiostat P20X8 ("Elins" LLC, Russia). In CV measurements, the potential range was 10–2000 mV with a sweep rate of 0.1 mV/s. GST was performed in two regimes: 1) with constant current throughout the whole cycling (0.1*C*); 2) with constant charge rate of 0.1*C* and different discharge rates of 0.1*C*, 0.2*C*, 0.3*C*, 0.5*C* and 1.0*C*. Intermediate discharge at 0.1*C* for 10 cycles between every 10 cycles with different discharge rates was used. (0.1*C* rate corresponded to 0.1 A g^{-1}; this value was estimated from the supposed capacity of the Si/RGO active mass equal to 1000 $mAh \cdot g^{-1}$).

Results and discussion

Scanning electron microscopy

Fig. 1 illustrates the morphology of the Si/RGO composite studied by scanning electron microscopy. RGO provides a flexible interconnected matrix in which agglomerated silicon nanoparticles are randomly distributed. SEM data demonstrate that some of the agglomerated Si nanoparticles occupy the surface positions, but most of them allocated between RGO sheets. As mentioned in Introduction, RGO sheets can enhance the stability of Si-based composite material during Li^+ insertion-extraction cycles since they provide fast electron transfer and mechanical support for silicon nanoparticles. Voids

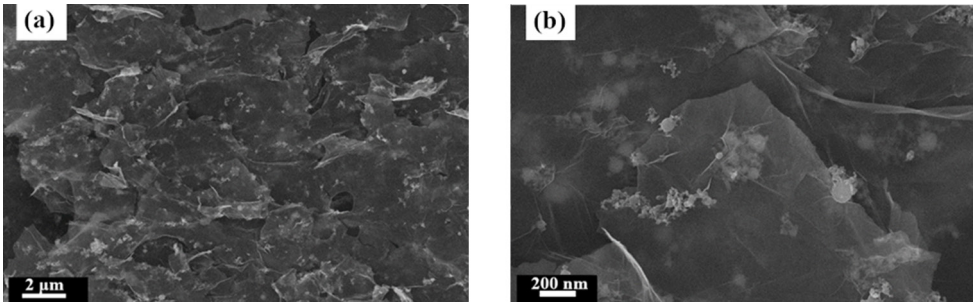

Fig. 1. Si/RGO composite SEM images with different magnifications

in the composite structure allow accommodating volume changes of silicon nanoparticles during cycling, thus stabilising the electrode.

Cyclic voltammetry

CV curves allow a better understanding of the electrochemical behaviour of the Si/RGO electrodes during cycling. Fig. 2 shows the initial three cycles for all samples under investigation. One can see that anode half-cells comprising Si/RGO electrodes with and without polymer binder demonstrated different electrochemical behaviour. For the SiRGO1 electrode without binder cathodic and anodic curves for the 1st, 2nd and 3rd cycle are practically the same. In contrast, for the SiRGO2 and SiRGO3 electrodes with a polymer binder, well-distinguishable peaks appear only in the second cycle and their intensity increases by the third cycle. The positions of the peaks are in good agreement with the literature data [16–19], according to which they can be attributed to the processes of insertion/extraction of lithium into silicon or RGO nanoparticles and to the SEI formation. Gradual appearance of the peaks on cycling (Fig. 2(b, c)) can be attributed to the influence of polymer binder on the surface chemistry of silicon particles distributed in the carbon matrix. CMC can bind with silicon surface by formation of ester or hydrogen bonds [9, 10],

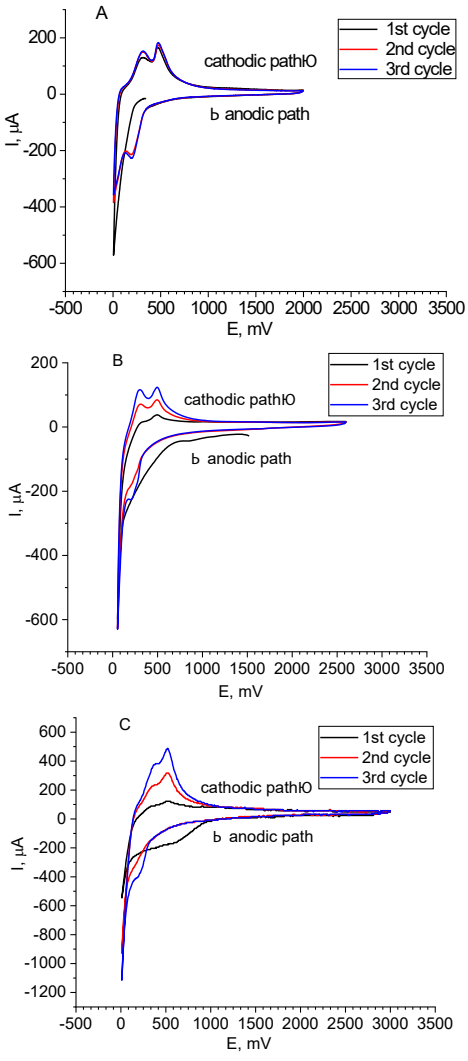

Fig. 2. Cyclic voltammograms of (A) SiRGO1; (B) SiRGO2; (C) SiRGO3

whereas PVdF forms with silicon surface Van-der-Vaals bonds only. Chemical bonds formation caused by CMC influences on the positions and intensity of the typical peaks.

Galvanostatic cycling

The electrochemical performance of anode half-cells comprising Si/RGO nanocomposites was studied by galvanostatic charge-discharge cycling in the range 10 to 2000 mV under the same conditions at room temperature. Fig. 3 shows the charge-discharge curves in the 1st, 2nd and 5th cycles for the cells with SiRGO1 (Fig. 3A), SiRGO2 (Fig. 3C) and SiRGO3 (Fig. 3E) electrodes. In the first cycle, the initial discharge capacities of the electrodes were 573 mAh·g^{-1}, 1350 mAh·g^{-1} and 249 mAh·g^{-1}, the values of the Coulomb efficiency were 56%, 69% and 21%, respectively. Table 2 summarises the electrochemical behaviour of electrodes based on Si/RGO nanocomposites with different binders.

The discharge curves of the 1st cycle are typical for formation cycles in LIBs. All the curves contain a step near 800 mV, which corresponds to the reduction of electrolyte components on the surface of active materials Si and RGO resulting in a protective SEI layer formation. This step disappeared in the next cycles (Fig. 3). Formation of SEI is the well-known reason for low Coulombic efficiency in the first cycle [7]. The enhanced surface electrochemical reactivity of Si/RGO nanocomposites must be attributed to the large surface-to-volume ratio of both RGO and Si [15, 20]. However, the sample SiRGO3 with CMC binder differ from others: one can see that the first discharge curve contains one more step near 1500 mV. This new process is responsible for the largest decrease in Coulomb efficiency at the first cycle (Table 2). Most likely, a polymer binder also participates in the reduction processes during the first cathodic polarisation of the Si/RGO electrode. This conclusion is in good agreement with the CV data.

As can be seen from Fig. 3 (B, D, F), the cyclic behaviour of the cell comprising SiRGO3 electrode is fundamentally different from others. Indeed, the capacity of electrodes without a polymer binder (SiRGO1, Fig. 3B) and with PVDF as a binder (SiRGO2, Fig. 3D) drops upon cycling, while the capacity of an electrode with a CMC binder (Fig. 3E) increases rapidly during the first 8 cycles and then stabilises near 1200 mAh·g^{-1} (Table 2).

The theoretical capacity of composite samples Si/RGO can be calculated based on the content of Si nanoparticles and RGO in the composite using their theoretical capacity. As was mentioned above, Si has the theoretical capacity of 3579 mAh·g^{-1} and graphene, by different evaluations, has the theoretical capacity ranging from 500 to 1116 mAh·g^{-1} [21]. The composite contained 50 mass % Si nanoparticles and 50 mass % RGO. The theoretical capacity (Q_{th}) of the composite is calculated using formula (1):

$$Q_{th} = Q_{Si} \cdot \omega_{Si} + Q_{RGO} \cdot \omega_{RGO}, \qquad (1)$$

where Q_{Si} and Q_{RGO} are theoretical capacities of Si and RGO, respectively; ω_{Si} and ω_{RGO} are mass fractions of Si and RGO in the composite, respectively. The resulting value of the theoretical capacity of the Si/RGO composite, using the minimum value of 500 mAh·g^{-1} as the theoretical capacity of RGO, was estimated as 2040 mAh·g^{-1}. As can be seen from Table 2, the capacity values of all samples under investigation fall below the theoretical one, which is typical for any Si-based anode materials [2–7].

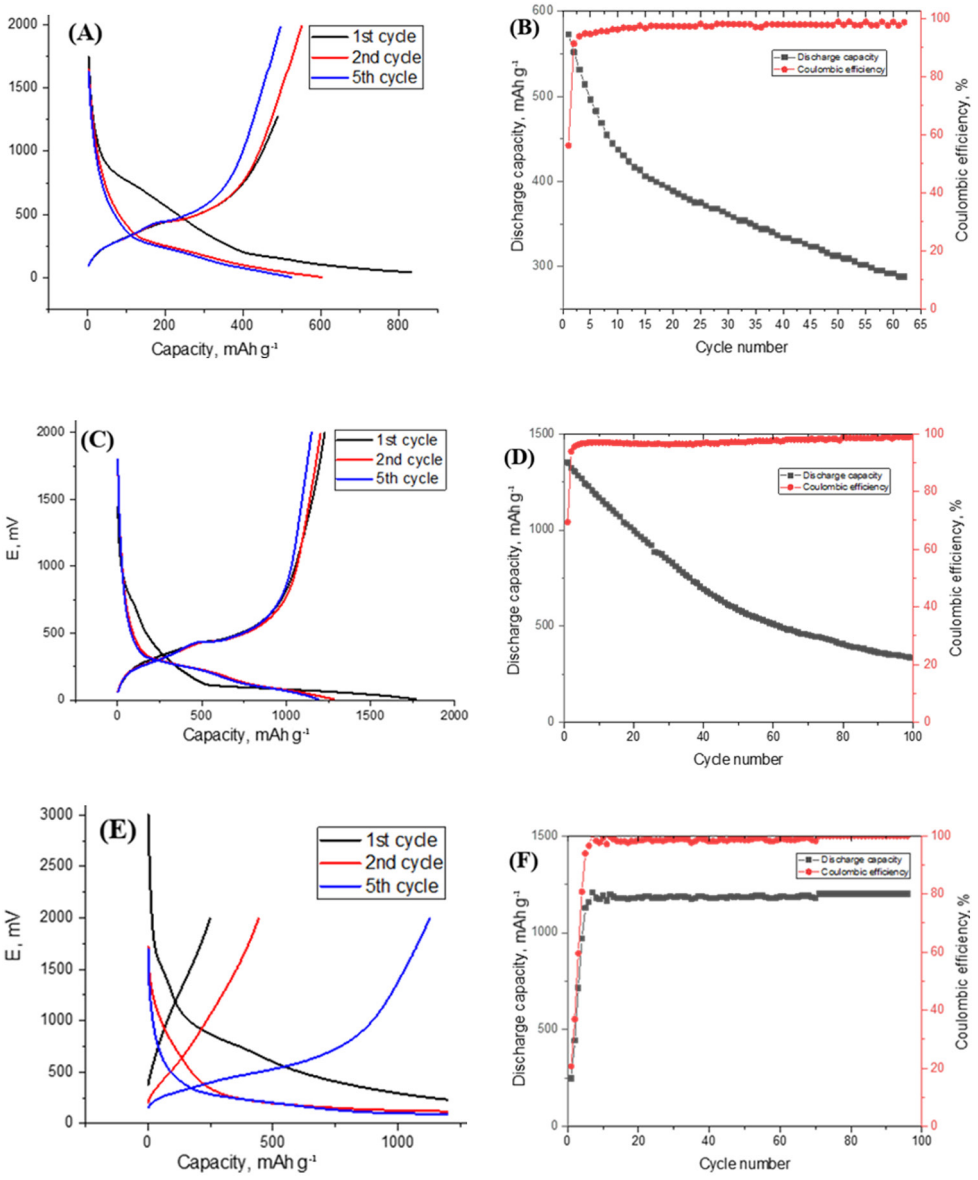

Fig. 3. Charge-discharge curves (A, C, E) and dependences of discharge capacity and Coulombic efficiency (B, D, F) on cycle number for SiRGO1 (A, B), SiRGO2 (C, D) and SiRGO3 (E, F)

Table 2

The cycle performance of the Si/RGO electrodes in the range of 0.01–2 V at 0.1*C* rate

Sample	Discharge capacity, mAh·g^{-1}			Coulombic efficiency, %			Capacity retention, %	
	1st cycle	60th cycle	100th cycle	1st cycle	60th cycle	100th cycle	60th cycle	100th cycle
SiRGO1	573	292	-	56	99	-	51	-
SiRGO2	1350	512	334	69	98	99	38	25
SiRGO3	249	1186	1200	21	99	100	100	100

As follows from the obtained results, CMC binder can solely enhance the stability of silicon-carbon nanocomposite. This conclusion is in line with those presented in [22]. In [23], authors declare that CMC alone is too brittle to effectively stabilise Si-based negative electrodes during cycling. However, in this work, CMC demonstrated excellent stabilisation properties. The observed effect can be attributed to the formation of hydrogen bonds between functional groups on the surface of silicon particles and carboxyl groups in CMC and between CMC carboxyl groups and residual functional groups in the surface of RGO nanosheets. Such bonds can be broken during volume expansion of silicon nanoparticles during lithiation and restored during delithiation thus preventing the material from the isolation of particles and helps maintain material integrity [10].

Rate capability was studied for the best SiRGO3 electrode; different discharge rates of 0.1*C*, 0.2*C*, 0.3*C*, 0.5*C* and 1.0*C* were used. Fig. 4 presents the results of these measurements. The first 10 cycles at 0.1*C* were used as the formation cycles. One can see that the SiRGO3 electrode shows good rate capability up to 1.0*C*, which can be attributed to both small silicon particle size (50 nm) and presence of conductive RGO layers which support fast electron transfer through the composite and enables high power operation of half-cell

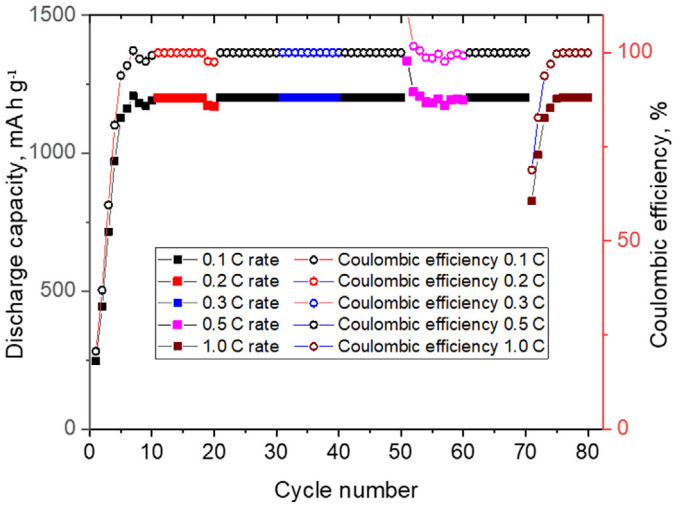

Fig. 4. Rate capability of the SiRGO3 electrode with CMC binder

[7]. The SiRGO3 electrode demonstrated the capacity of ~1200 mAh·g^{-1} at any discharge rate with the exception of 1.0*C*. At 1.0*C*, the electrode capacity reached ~1200 mAh·g^{-1} only at the 4th cycle. Perhaps this is due to some diffusion difficulties or rearrangement of the conducting paths. However, after that, the capacity again stabilised at the ~1200 mAh·g^{-1} value. Some anomalies were also observed at 0.5C, when the capacity first deviated towards higher values causing Coulombic efficiency above 100%, and then stabilised at the previous level of 1200 mAh·g^{-1}. The reasons for this behaviour are unclear and require additional examination.

Conclusions

Polymer binder plays a crucial role in stabilising the Si/RGO nanocomposite material during cycling. The electrode with PVdF binder demonstrated better initial Coulombic efficiency of 69%, but the exponential capacity loss was observed down to capacity retention 25% after 100 cycles. The electrode with CMC binder exhibited low initial Coulombic efficiency of 21% due to additional reduction process with binder participation. However, the resulting SEI provided stable cycling with discharge capacity near 1200 mAh·g^{-1} and 100% capacity retention after 100 cycles at 0.1*C*. Excellent rate capability up to 1.0*C* with no capacity fade during cycling was also observed.

Acknowledgements

This work was performed with financial support from the Ministry of Science and Higher Education of Russian Federation, project ID RFMEFI60419X0235.

References

1. Asenbauer J, Eisenmann T, Kuenzel M, Kazzazi A, Chen Z, Bresser D. The success story of graphite as a lithium-ion anode material — fundamentals, remaining challenges, and recent developments including silicon (oxide) composites. Sustain Energy Fuels. 2020;4(11):5387–416. doi:10.1039/D0SE00175A
2. Chae S, Choi S-H, Kim N, Sung J, Cho J. Integration of graphite and silicon anodes for the commercialization of high-energy lithium-ion batteries. Angew Chem Int Ed Engl. 2020;59(1):110–35. doi:10.1002/anie.201902085
3. Obrovac MN, Christensen L. Structural changes in silicon anodes during lithium insertion/extraction. Electrochem Solid State Letters. 2004;7(5):A93. doi:10.1149/1.1652421
4. Luo F, Liu B, Zheng J, Chu G, Zhong K, Li H, et al. Review — nano-silicon/carbon composite anode materials towards practical application for next generation Li-ion batteries. J Electrochem Soc. 2015;162(14):A2509–28. doi:10.1149/2.0131514jes
5. Wu H, Cui Y. Designing nanostructured Si anodes for high energy lithium ion batteries. Nano Today. 2012;7(5):414–29. doi:10.1038/35104644

6. Su X, Wu Q, Li J, Xiao X, Lott A, Lu W, et al. Silicon-based nanomaterials for lithium-ion batteries: A review. Adv Energy Mater. 2014;4(1):1300882. doi:10.1002/aenm.201300882
7. Shi Q, Zhou J, Ullah S, Yang X, Tokarska K, Trzebicka B, et al. A review of recent developments in Si/C composite materials for Li-ion batteries. Energy Storage Mater. 2021;34:735–54. doi:10.1016/j.ensm.2020.10.026
8. Wu J, Cao Y, Zhao H, Mao J, Guo Z. The critical role of carbon in marrying silicon and graphite anodes for high-energy lithium-ion batteries. Carbon Energy. 2019;1(1):57–76. doi:10.1002/cey2.2
9. Lestriez B, Bahri S, Sandu I, Roue L, Guyomard D. On the binding mechanism of CMC in Si negative electrodes for Li-ion batteries. Electrochem commun. 2007;9(12):2801–6. doi:10.1016/j.elecom.2007.10.001
10. Istomina AS, Bushkova OV. Polimernye svyazuyushchie dlya elektrodov litievykh akkumulyatorov chast' 1. Polivinilidenftorid, ego proizvodnye i drugie kommertsializovannye materialy [Polymer binders for the electrodes of lithium batteries. Part 1. Polyvinylidene fluoride, its derivatives and other commercialized materials]. Elektrokhimicheskaya energetika [Electrochemical Energetics]. 2020;20(3):115–131. Russian. doi:10.18500/1608-4039-2020-20-3-115-131
11. Zhou X, Yin Y-X, Wan L-J, Guo Y-G. Self-assembled nanocomposite of silicon nanoparticles encapsulated in graphene through electrostatic attraction for lithium-ion batteries. Adv Energy Mater. 2012;2(9):1086–90. doi:10.1002/aenm.201200158
12. Ding N, Chen Y, Li R, Chen J, Wang C, Li Z, et al. Pomegranate structured C@pSi/rGO composite as high performance anode materials of lithium-ion batteries. Electrochim Acta. 2020;(137491):137491. doi:10.1016/j.electacta.2020.137491
13. Agyeman DA, Song K, Lee G-H, Park M, Kang Y-M. Carbon-coated Si nanoparticles anchored between reduced graphene oxides as an extremely reversible anode material for high energy-density Li-ion battery. Adv Energy Mater. 2016;6(20):1600904. doi:10.1002/aenm.201600904
14. Botas C, Carriazo D, Zhang W, Rojo T, Singh G. Silicon-reduced graphene oxide self-standing composites suitable as binder-free anodes for lithium-ion batteries. ACS Appl Mater Interfaces. 2016;8(42):28800–8. doi:10.1021/acsami.6b07910
15. Novikov D. V., Evschik E. Yu., Berestenko V. I., Yaroslavtseva T. V., Levchenko A. V., Kuznetsov M. V., Bukun N. G., Bushkova O. V., Dobrovolsky Yu. A. Electrochemical performance and surface chemistry of nanoparticle Si@SiO_2 Li-ion battery anode in $LiPF_6$-based electrolyte. Electrochimica Acta 2016;208:109–119. doi:10.1016/j.electacta.2016.04.179

16. Tokur M, Algul H, Ozcan S, Cetinkaya T, Uysal M, Akbulut H. Closing to scaling-up high reversible Si/rGO nanocomposite anodes for lithium ion batteries. Electrochim Acta. 2016;216:312–9.
doi:10.1016/j.electacta.2016.09.048
17. Zhai W, Ai Q, Chen L, Wei S, Li D, Zhang L, et al. Walnut-inspired microsized porous silicon/graphene core — shell composites for high-performance lithium-ion battery anodes. Nano Res. 2017;10(12):4274–83.
doi:10.1007/s12274-017-1584-5
18. Ogata K, Salager E, Kerr CJ, Fraser AE, Ducati C, Morris AJ, et al. Revealing lithium-silicide phase transformations in nano-structured silicon-based lithium ion batteries via in situ NMR spectroscopy. Nat Commun. 2014;5(1):3217.
doi:10.1038/ncomms4217.
19. Feng J, Zhang Z, Ci L, Zhai W, Ai Q, Xiong S. Chemical dealloying synthesis of porous silicon anchored by in situ generated graphene sheets as anode material for lithium-ion batteries. J Power Sources. 2015;287:177–83.
doi:10.1016/j.jpowsour.2015.04.051
20. Szczech JR, Jin S. Nanostructured silicon for high capacity lithium battery anodes. Energy Environ Sci. 2011;4(1):56–72.
doi:10.1039/C0EE00281J
21. Kheirabadi N., Shafiekhani A. Graphene/Li-ion battery. J Appl Phys. 2012;112(12):124323.
doi:10.1063/1.4771923
22. Xiao J, Xu W, Wang D, Choi D, Wang W, Li X, et al. Stabilization of silicon anode for Li-ion batteries. J Electrochem Soc. 2010;157(10):A1047.
doi:10.1149/1.3464767
23. Casimir A, Zhang H, Ogoke O, Amine JC, Lu J, Wu G. Silicon-based anodes for lithium-ion batteries: Effectiveness of materials synthesis and electrode preparation. Nano Energy. 2016;27:359–76.
doi:10.1016/j.nanoen.2016.07.023